Research Square

Preprints are preliminary reports that have not undergone peer review.
They should not be considered conclusive, used to inform clinical practice,
or referenced by the media as validated information.

Evaluation of Fabrication Techniques on the Mechanical Properties and Microbial Adhesion of PMMA-Based Dentures：An In Vitro Study

Shuobo Fang
Shanghai Stomatological Hospital & School of Stomatology, Fudan University
Yilin Tu
Shanghai Stomatological Hospital & School of Stomatology, Fudan University
Nuoyan Xu
Shanghai Stomatological Hospital & School of Stomatology, Fudan University
Zhe Shen
Shanghai Xuhui District Stomatological Hospital
Zhicheng Gong
Shanghai Stomatological Hospital & School of Stomatology, Fudan University
Jue Wang
Shanghai Stomatological Hospital & School of Stomatology, Fudan University
Xueying Wu
Shanghai Stomatological Hospital & School of Stomatology, Fudan University
Taoran Qu
qutaoran@163.com
Shanghai Stomatological Hospital & School of Stomatology, Fudan University

Research Article

Keywords: Polymethyl methacrylate, Injection molding, 3D printing, CAD/CAM milling, Mechanical Properties, Microbial colonization

Posted Date: November 12th, 2026

DOI: https://doi.org/10.21203/rs.3.rs-11478290/v1

License: This work is licensed under a Creative Commons Attribution 4.0 International License.
Read Full License

Additional Declarations: No competing interests reported.

Evaluation of Fabrication Techniques on the Mechanical Properties and Microbial Adhesion of PMMA-Based Dentures：An In Vitro Study

Shuobo Fang[1#], Yilin Tu[2#], Nuoyan Xu[3], Zhe Shen[4], Zhicheng Gong[3], Jue Wang [1], Xueying Wu[1], Taoran Qu[1*]

[1] Department of Prosthodontics, Shanghai Stomatological Hospital & School of Stomatology, Shanghai Key Laboratory of Craniomaxillofacial Development and Diseases, Fudan University, Shanghai, PR China

[2] Department of Implantology, Shanghai Stomatological Hospital & School of Stomatology, Shanghai Key Laboratory of Craniomaxillofacial Development and Diseases, Fudan University, Shanghai, PR China

[3] Department of Dental Technology, Shanghai Stomatological Hospital & School of Stomatology, Fudan University, Shanghai, PR China.

[4] Department of Periodontology, Shanghai Xuhui District Stomatological Hospital, Shanghai, PR China.

#These authors contributed equally to this work

*** Corresponding author:**

Dr Taoran Qu

Department of Prosthodontics，Shanghai Stomatological Hospital & School of Stomatology, Shanghai Key Laboratory of Craniomaxillofacial Development and Diseases, 160 Hechuan Rd, Minhang District, Shanghai, 2000, China

E-mail: qutaoran@163.com

ABSTRACT

Objective: To investigate the impact of three fabrication techniques, including injection molding, three-dimensional (3D) printing, and milling, on the mechanical properties and microbial colonization of PMMA based dentures.

Material and methods: Three groups of PMMA specimens were fabricated (n=30), Group I (injection molding), Group P (3D printing), and Group M (CAD/CAM milling), respectively. Three-point bending tests were conducted to determine flexural strength, flexural modulus, stress-strain curves and Weibull distribution of three groups, of which half (n=15) underwent 10,000 thermocycles before testing. Scanning electron microscope (SEM) was applied to observe the fracture surfaces. Surface roughness was quantified with atomic force microscopy (AFM). Microbial colonizations of *Candida albicans* (*C. albicans*) and *Streptococcus oralis* (*S. oralis*) were quantified via colony-forming unit (CFU) assays. Data were analyzed using independent samples t-tests and one-way analysis of variance (ANOVA) ($\alpha = 0.05$).

Results: Group I showed greatest decrease in flexural strength after thermocycling ($p<0.05$). Group P exhibited the highest flexural strength before thermocycling and a significant reduction after thermocycling ($p<0.05$). Group M retained the most stable mechanical performance. Surface roughness was comparable across groups ($p>0.05$). Group P showed the highest number of colonies for *C. albicans* and *S. oralis*. ($p<0.05$).

Conclusions: Fabrication techniques affects properties of PMMA based dentures. Milled PMMA dentures offer greater long-term durability. 3D-printed dentures exhibit great mechanical properties but higher microbial colonization.

Clinical Significance: Clinicians should balance mechanical durability and microbial susceptibility when selecting fabrication techniques for patients.

Keywords: Polymethyl methacrylate, Injection molding, 3D printing, CAD/CAM milling, Mechanical Properties, Microbial colonization

1. Introduction

Polymethyl methacrylate (PMMA) has remained the predominant material for complete denture bases since mid-1940s attributed to its favorable biocompatibility, aesthetics, and clinical manipulability(1). The clinical longevity and performance of these prostheses are not solely determined by the material itself but are also critically dependent on the fabrication technology employed.

Conventional heat-polymerized PMMA, synthesized via the free-radical polymerization of powder-liquid monomers, often suffers from inherent limitations such as polymerization shrinkage, residual internal stress, and operator-dependent variability(2). Consequently, these dentures are prone to fractures and dimensional inaccuracies in terms of long-term performance.

Digital processing techniques include subtractive manufacturing and additive manufacturing(3). Subtractive manufacturing utilizes pre-polymerized PMMA blocks, offering superior density and mechanical stability. Helal et al. confirmed that milling system in complete denture fabrication showed superior dimensional accuracy than additive manufacturing systems and the compression molding system(4). However, this method is constrained by high material waste, tool geometry restrictions, and elevated costs.

Additive manufacturing enables the fabrication of complex undercut geometries with minimal material consumption and high workflow efficiency(5) (6). Nevertheless, layer-by-layer fabrication introduces anisotropic properties and potential dimensional errors influenced by printing parameters and post-curing protocols(7). Photocurable resins relies on incorporated photo initiators(8), while the degree of cross-linking must be carefully controlled, as excessive cross-linking can increase brittleness despite improving surface hardness(9). To enhance flexural strength, three-dimensional (3D) printing PMMA resins are often modified with particulate fillers. Although such reinforcement is conducive to meet mechanical demands, it may alter fracture behavior and influence microbial colonization patterns(10, 11). Besides, support structures for 3D printing need post-print polishing that compromises the fabrication accuracy(12).

From a physicochemical perspective, the conversion of methyl methacrylate (MMA) monomers into high-molecular-weight polymer networks dictates the final mechanical properties(1). Incomplete polymerization leads to residual monomer leaching, which is a known etiological factor for mucosal irritation and denture stomatitis(13). Microbial colonization to PMMA based dentures is influenced by

material attributes, including chemical composition and surface characteristics(14). Surface characteristics, such as surface roughness and surface area, regulate the colonization of pathogens like *Candida albicans* (*C. albicans*) and *Streptococcus oralis* (*S. oralis*), exacerbating biofilm formation and compromising both tissue health and material integrity(15-17).

It remains a consideration to achieve a balance between mechanical properties and microbial colonization in modern denture base PMMA development/denture base fabrication. Yu et al. reported that 3D printing PMMA outperformed conventional and milling resins in flexural strength and flexural modulus, confirming its excellent mechanical suitability for denture bases(4). When it comes to microbial colonization, Koujan et al. (18) reported approximately twofold greater *C. albicans* colonization on 3D printing than on milling or heat-curing PMMA. Hougne et al. (15) found milled PMMA accumulated less *Streptococcus sanguinis* biofilm than both 3D printing and conventionally processed materials. Some investigators demonstrated that computer-aided-design/computer-aided-manufacturing (CAD/CAM) milling yields lower initial flexural strength, its industrially pre-polymerized blocks produce near-zero-porosity surfaces that resist microbial colonization(14, 19). Therefore, a comprehensive evaluation integrating both mechanical reliability and microbial susceptibility is warranted to guide clinical material selection.

This study aims to evaluate the mechanical properties and microbial colonization of PMMA denture base materials used in injection molding, CAD/CAM milling, and 3D printing. Denture bases withstand repeated masticatory forces in long-term use. Therefore, flexural strength and flexural modulus are applied to reflect the fracture resistance of denture bases. Since the fracture of denture base always occurs from the weak area, the Weibull distribution was analyzed to assess the reliability and lifetime of PMMA. Moreover, fabrication techniques may influence microbial colonization by material ingredients and the surface topography of PMMA, so the colonization of typical microorganisms were counts. The null hypothesis was that there were no differences regarding these indicators among the three PMMA denture base materials.

2. Materials and methods

2.1. Mechanical Characterization

2.1.1 Specimen Preparation

All specimens were prepared according to ISO 20795-1-2013 standard(20). Three groups of specimens were fabricated by three techniques with their corresponding PMMA denture base materials, including Group I (Injection molding), Group P (3D printing) and Group M (CAD/CAM milling). Thirty specimens were standardized to identical dimensions of 65mm×40mm×3.3mm for each group. The mechanical properties tests workflow chart is presented in Fig. 1. and the detailed specifications and manufacturers of the materials used in each group are listed in Table 1. The specimen preparation processes for three techniques are as follows:

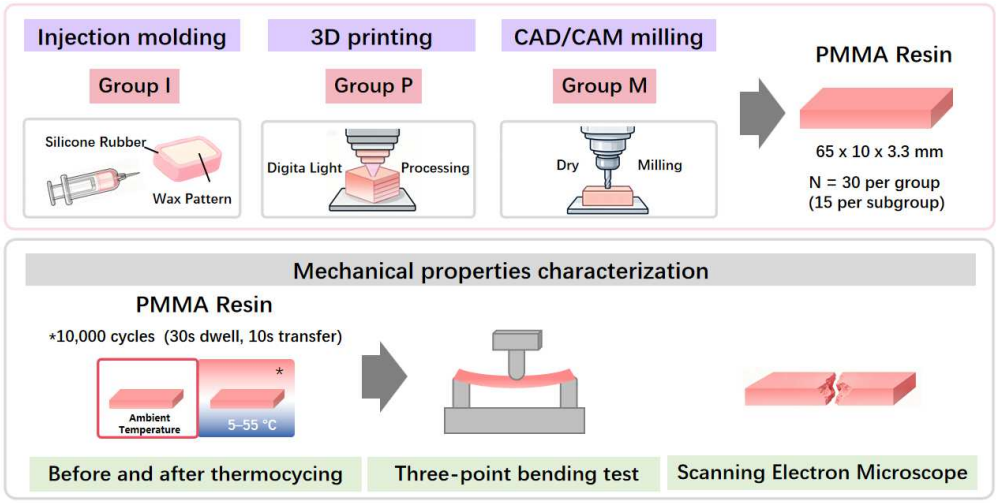


Fig. 1. The workflow chart of mechanical properties tests.

A rectangular block model was designed using Materialise Magics 27.0 software (Materialise, Leuven, Belgium) and exported in the standard tessellation language (STL) format.

Group I: A wax pattern was milled from the was disk (Wax Disk, Shanghai Huliang Biomedical Technology Co., Ltd, China) based on the block model data and embedded step-by-step using silicone rubber (Titanium, Zhermack SpA, Italy). One half was embedded first, followed by the remaining half after the silicone rubber had solidified. The silicone mold was then separated to remove the internal wax pattern. Since injection channels had been reserved during embedding, the injection molding material (Vertex-Self Curing, Vertex Co., Ltd., Netherland) was finally injected into the mold cavity with a syringe to form the specimens.

Group P: The specimens were printed from the block model data via a digital light processing (DLP) 3D printer (Pro 95 S, SprintRay Inc., USA) with a light-curable denture base material (High Impact Denture Base, SprintRay Inc., USA) according to

manufacturer's recommended protocols. The printing parameters included a layer thickness of 0.1mm, a printing light source wavelength of 405nm, and resolutions of 0.095mm on the X-axis, 0.095mm on the Y-axis, and 0.01mm on the Z-axis. After printed, they were ultrasonically cleaned twice in 95% isopropyl alcohol for 2 min each time, then blow-dried. Post-curing was performed using a curing unit (Procure 2, SprintRay Inc., USA) at a wavelength of 385nm with a light intensity ≥ 40mW/cm^2, a curing temperature of 50℃, and a curing time of 5min. After cooling, the supports were removed, and the specimens were grinded and polished.

Group M: The pre-polymerized PMMA disks (Removable Denture (mono), Shanghai Huliang Biomedical Technology Co., Ltd, China) were secured in a milling machine (Xiangtong MILL-600, Shenzhen Xiangtong Optoelectronic Technology Co., Ltd., China). After calculating the cutting path from the block model data, the specimens were obtained by dry milling to complete the fabrication.

Table 1. Materials used in this study.

Group	**Product**	**Manufacturer**	**Nation**	**Material composition (main Components)**
Group I	Vertex-Self Curing	Vertex Co., Ltd.	Netherland	Powder: Poly (methyl methacrylate), benzoyl peroxide; Liquid: Methyl methacrylate, N,N-dimethyl-p-toluidine, ethylene glycol dimethacrylate
Group P	SprintRay High Impact Denture Base	SprintRay Inc.	USA	Silicon dioxide (nanofiller, 19.9 ± 1.1%)(21) *Note: Proprietary components not disclosed.*

Group M	Removable Denture (mono)	Shanghai Huliang Biomedical Technology Co., Ltd.	China	Polymethyl methacrylate, Methyl methacrylate, Butyl methacrylate

Composition comes from manufacturer's safety data sheet and product technical document.

All specimens were then prepared to the final size. First of all, a low-speed cutting machine (SYJ-150, Shenyang Kejing Automation Equipment Co., Ltd., China) was used to mill each specimen into equal length and thus there were thirty specimens per group, measuring 65 mm × (10.0 ± 0.2) mm × (3.3 ± 0.2) mm, ensuring that the dimensions were slightly larger than the specified dimensions. Besides, specimens were sequentially sanded using 800, 1200, 2000 and 3000-grit water-resistant silicon carbide sandpaper under running water, followed by polishing with a polishing compound (water-soluble diamond polishing paste W2.5, Shenyang Kejing Automation Equipment Co., Ltd., China) until the surface became glossy. Then, a micrometer was used to measure three points along the long axis of each test strip to determine its height, with an accuracy of 0.01 mm. Dimensional tolerances were maintained within ± 0.02 mm for flat and of uniform height. The test specimens were ultrasonically cleaned for 5 minutes, followed by blow-drying and stored prior to use.

2.1.2 Three-point bending test

Thirty specimens per group were randomly allocated into two subgroups (n = 15). One subgroup underwent 10,000 cycles of thermocycling at 5-55°C with a 30 seconds dwell time and 10 seconds transfer time, while the other subgroup was stored at room temperature until testing. Width and thickness were measured in triplicate, and means were calculated for each specimen. Three-point bending tests were performed on a test fixture with a span of 50 mm in a universal testing machine (EZ-SX 500N, Shimadzu, Japan). In accordance with ISO 20795-1-2013 standard(20), vertical downward loading was applied at a crosshead speed of 5.0 mm/min until fracture occurred, and the maximum fracture load was recorded.

2.1.3 SEM

Specimens were cut from fractured surfaces of Group I, Group P, and Group M, placed in 10 mL of 95% isopropyl alcohol and sonicated at 40KHz (SB25-12DT, NingBo XinZhi Biotechnology Co., Ltd, China) for 5 min. Then, all specimens were sputter-coated with a 100 nm platinum layer using an ion sputter coater (MC1000, Hitachi, Japan). Subsequently, typical surface micromorphology images were observed and captured using a field-emission scanning electron microscope (Regulus 8100, Hitachi, Japan) at gradient magnifications ranging from 1000 to 50,000 times.

2.2 Surface characterization and Microbial colonization

2.2.1 Water contact angle

Five new specimens for each group were ultrasonically cleaned with anhydrous ethanol for 15 minutes, rinsed with deionized water, and then dried in a clean container for 20 minutes. A contact angle measuring instrument (SDC-350, ShengDing, China) was applied and a 10μL test droplet was deposited on the surface using a micro–syringe. Image capture was completed within 5 seconds after the droplet reached a stable state. The left and right contact angles were calculated with the Laplace-Young fitting method.

2.2.2 Atomic force microscope (AFM)

Surface morphology and roughness of the denture base specimens were evaluated using AFM. Disk-shaped specimens with a diameter of 9 mm and a thickness of 2 mm were prepared from the three material groups including Group I, Group P and Group M. Both surfaces of each specimen were examined. AFM imaging was performed using a Bruker Dimension Icon system (Bruker, Germany). Before imaging, the probe was mounted, followed by laser alignment, photodetector adjustment, tip positioning, and focusing on the specimen surface. After the initial scanning parameters were checked, surface images were acquired and saved for subsequent roughness analysis.

2.2.3 Microbial colonization

Microbiological test specimens with the dimensions of 10 mm in diameter × 2 mm in height were prepared using the same protocol as for mechanical characterization. Three PMMA-based groups with 10 per group were prepared. To accurately reflect the biological performance of the tissue surface of dentures in clinical scenarios(22), no

grinding or polishing treatment was applied on these specimens.

The colony counting method was employed to compare the effects of three PMMA groups on the colonization of *C. albicans* (ATCC 90028, China General Microbiological Culture Collection Center, China) and *S. oralis* (ATCC 9811, Shanghai Pufei Biotech Co., Ltd, China). First, all specimens were sterilized by soaking in 75% ethanol for 10 min followed by 10 min of ultraviolet irradiation and were then reserved for subsequent use. After activation on agar plates, the two microbial strains were inoculated separately into brain heart infusion (BLI) (Oxoid CM1135B, Thermo Fisher Scientific Inc., UK) at 37°C in an atmosphere of 5% CO_2 for overnight culture. Next day, microbial cells were harvested, resuspended, and adjusted to an OD_{600} of 1.0. According to the conversion based on bacterial suspension concentration, *S. oralis* was further diluted to 2×10^6 CFU/mL, while *C. albicans* was diluted to 2×10^5 CFU/mL.

Subsequently, 1 mL of standardized bacterial suspension was added to each denture base specimen, followed by incubation at 37°C in an atmosphere of 5% CO_2 for 24 h. After incubation, the specimens were gently washed three times with Dulbecco's Phosphate-Buffered Saline (DPBS) (21-031-CV, Corning, USA) to remove non-adhered microorganisms. The specimens were then placed in 1 mL of DPBS and sonicated at 40KHz (SB25-12DT, NingBo XinZhi Biotechnology Co., Ltd, China) for 5 min to detach the microorganisms adhered to the surface. The obtained suspension was serially diluted and spread onto BHI agar plates (Oxoid LP0011B, Thermo Fisher Scientific Inc., UK). After incubation until colony formation, the plates were photographed and colony forming units were counted.

The samples were fixed with 2.5% glutaraldehyde at 4°C overnight and subsequently washed twice with HEPES buffer. Samples were dehydrated through a graded ethanol series (30%, 50%, 70%, 90%, and 100%; 5 min each), followed by an additional dehydration step in absolute ethanol. The specimens were then immersed twice in hexamethyldisilazane (HMDS) for 1 min each and allowed to dry overnight under fume hood. Finally, SEM imaging was performed and surface images were acquired.

2.3. Statistical analysis

Before analysis, Grubbs' test(23) was employed to rigorously screen for outliers in each group at the significance level of α=0.05. Flexural strength and flexural modulus were statistically analyzed using IBM SPSS Statistics 27 (IBM, USA) and Microsoft Excel (Microsoft Corporation, USA). GraphPad Prism 10.1.2 (GraphPad Software, USA). Independent samples t-tests was applied to compare flexural strength and modulus before and after thermocycling. Weibull analysis was performed via probability plotting of OriginPro 2021 (OriginLab, USA) at a 95% confidence level. A one-way analysis of variance (ANOVA) was conducted to surface roughness by IBM SPSS Statistics 27. The significance level was set at $\alpha = 0.05$.

3. Results

3.1 Flexural Strength and Flexural Modulus

The flexural strength of one specimen in Group I before thermocycling was identified as an outlier by Grubbs' test ($\alpha = 0.05$)(23) and was removed. Before thermocycling, Group P exhibited the highest flexural strength (130.29 ± 24.25 MPa, coefficient of variation (CV) = 18.61%), followed by Group I (101.87 ± 5.55 MPa, CV = 5.45%), while Group M recorded the lowest value (100.01 ± 7.93 MPa, CV = 7.93%). After thermocycling, different numerical trends were observed among the groups. Group P maintained the highest flexural strength (108.29 ± 20.91 MPa, CV = 19.31%). Group I showed the largest reduction, dropping to 72.18 ± 7.46 MPa (CV = 10.35%), which was the lowest value among all groups. Group M retained a flexural strength of 87.45 ± 7.78 MPa (CV = 8.90%). These differences before and after thermocycling were statistically significant for all groups ($p < 0.05$), as indicated by the asterisks in Fig.2 and Table 2. Specifically, Group I showed the most substantial decrease.

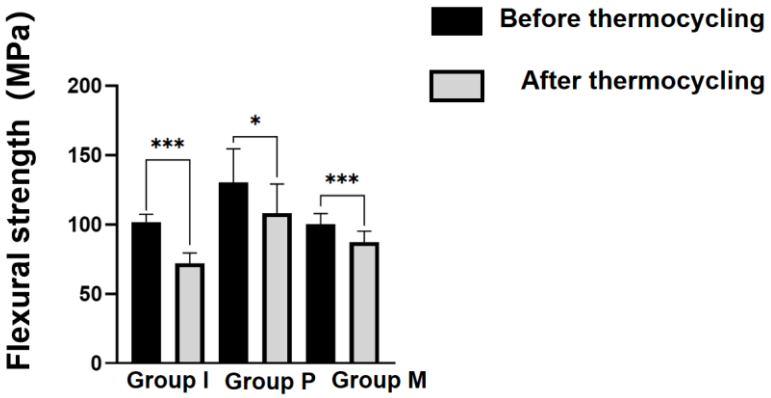


Fig. 2. Comparison of flexural strength for three fabrication techniques, Group I, Group P, and Group M before and after thermocycling.

Table 2. The flexural strength among three groups before and after thermocycling (MPa)

Group	Thermocycling	N	Mean ± SD	Coefficient of Variation	Width	Thickness	*P Value*
Group I	Before	14	101.87 ± 5.55	5.45	10.00 ± 0.11	3.34 ± 0.10	<0.001
	After	15	72.07 ± 7.46	10.35	10.07 ± 0.12	3.22 ± 0.07	
Group P	Before	15	130.29 ± 24.25	18.61	9.97 ± 0.11	3.28 ± 0.11	0.013
	After	15	108.29 ± 20.91	19.31	10.12 ± 0.10	3.31 ± 0.10	
Group M	Before	15	100.01 ± 7.93	7.93	9.99 ± 0.12	3.31 ± 0.08	<0.001
	After	15	87.45 ± 7.78	8.90	10.02 ± 0.07	3.33 ± 0.07	

Span Length：50mm

The flexural modulus of one specimen in Group I before thermocycling was identified as an outlier by Grubbs' test ($\alpha = 0.05$) (23) and was removed. The results of flexural modulus indicated that different groups exhibited distinct variation trends in flexural modulus following thermocycling. Before thermocycling, Group P exhibited the highest flexural modulus 2.8 ± 0.12 GPa, followed by Group M 2.78 ± 0.12 GPa, while Group I recorded the lowest value 2.18 ± 0.22 GPa. After thermocycling, Group M became the highest flexural modulus 2.4 ± 0.09 GPa. The flexural modulus of Group I increased to 2.31 ± 0.07 GPa. Group P exhibited the most pronounced reduction, reaching a value of 1.71 ± 0.17 GPa after thermocycling, which is the lowest among all tested groups.

According to the independent samples t-test, thermocycling induced a slight increase in Group I ($p = 0.048$), whereas Group P and Group M exhibited obvious reductions ($p < 0.05$) (Fig. 3, Table 3).

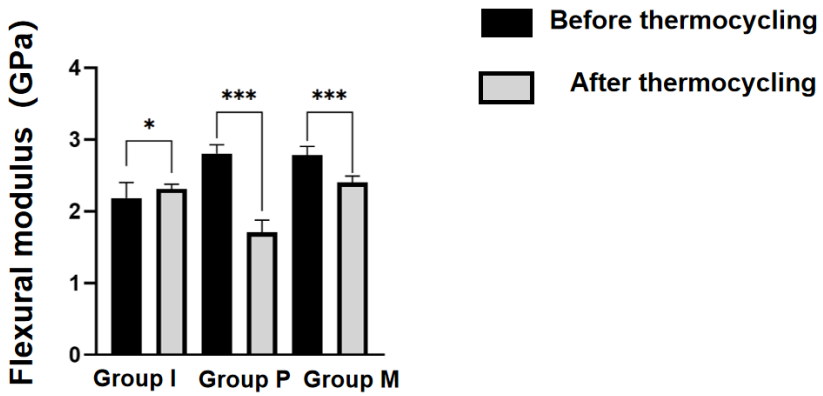


Fig. 3. Comparison of flexural modulus for three fabrication techniques, Group I, Group P, and Group M before and after thermocycling.

Table 3. The flexural modulus among three groups before and after thermocycling (GPa)

Group	Thermocycling	N	Mean ± SD	*P* Value
Group I	Before	14	2.18 ± 0.22	0.048
	After	15	2.31 ± 0.07	
Group P	Before	15	2.8 ± 0.12	<0.001
	After	15	1.71 ± 0.17	
Group M	Before	15	2.78 ± 0.12	<0.001
	After	15	2.4 ± 0.09	

Span Length：50mm

3.2 Stress-Strain Curve

As is shown in Fig. 4A1, Group I exhibited elastic deformation at the first stage before thermocycling, where stress was linearly proportional to strain. Plastic deformation that stress mainly brought the PMMA strain was observed at the second stage until a sudden fracture occurred at the third stage. Fluctuations appeared in some specimens during the early stages of loading. Most specimens fractured within a strain range of 4%-6%, displaying brittle fracture behavior without noticeable strain hardening prior to failure. A single specimen displayed ductile fracture behavior. After thermocycling, the strain at break shifted to 3%-4%, indicating a pronounced tendency toward brittle fracture (Fig. 4B1). Group M exhibited a similar fracture process with Group I before and after thermocycling (Fig. 4A1, B1, A3, B3), in which there were little fluctuations at the early stage.

Group P also exhibited linear elastic deformation at the first stage before thermocycling (Fig. 4A1). All specimens reached a yield plateau with the yield strength located in 90 MPa-100 MPa at the second stage. Upon surpassing the yield point, the material underwent a steep strain-hardening peak where the stress experienced a surge increase within the strain range of 6.5%-7.6% at the third stage. Subsequently, the curves displayed a strain-softening behavior that the stress required for further deformation decreased with a faster increase in strain at the fourth stage. Finally, fractured occurred at the fifth stage. After thermocycling, the yield plateau fell to 60 MPa and 70 MPa (Fig. 4B2).

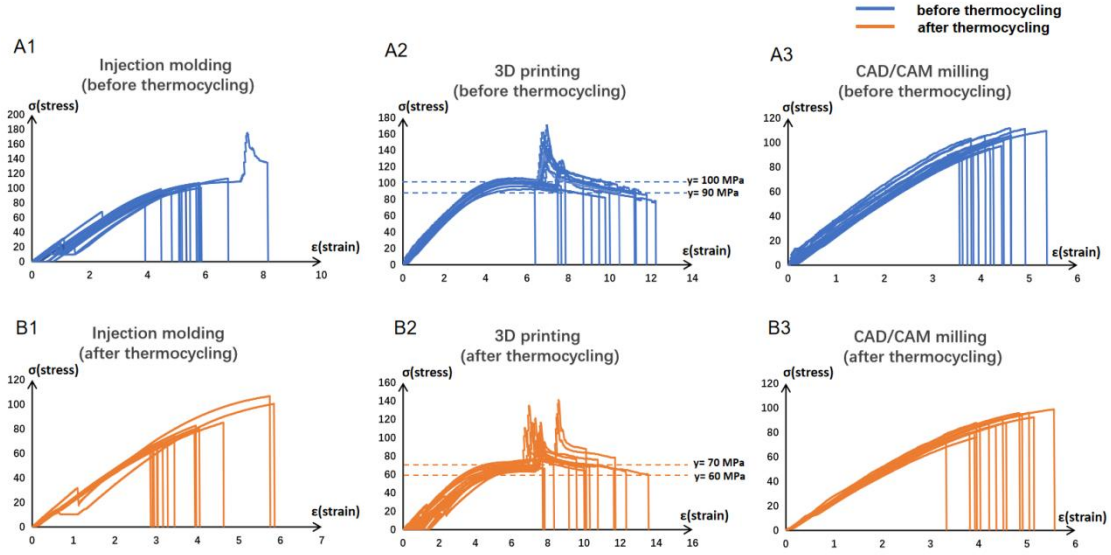


Fig. 4. Stress-strain curve for three fabrication techniques, A1), B1) all curves for Group I before and after thermocycling; A2), B2) for Group P; A3), B3) for Group M

3.3 Weibull distribution

Weibull analysis was performed on the flexural strength data of each group to assess the probability of PMMA failure through obtaining the shape parameter reflecting the mechanical stability and the scale parameter reflecting the characteristic fracture strength at 63.2% percentage. The specific probability distribution curves were presented in Fig. 5.

Before thermocycling, the measuring points of Group I were distributed in the range from 90 MPa to 120 MPa. The shape parameter of Group I was 19.76, and the scale was 104.42 MPa (Fig. 5A1). For Group P, the measurement points exhibited a wide distribution span, ranging from 95 MPa to 170 MPa. The shape parameter was 6.29, and the scale was 140.15 MPa (Fig. 5A2). The measuring points of Group M were

distributed in the range from 85 MPa to 115 MPa. The shape parameter was 14.80, and the scale was 103.56 MPa (Fig. 5A3). Overall, strength stability was highest in Group I, followed by Group M, with Group P being the lowest. The characteristic fracture strength was highest in Group P, followed by Group I, with Group M being the lowest.

After thermocycling, the scale parameter declined across all groups. Notably, Group I exhibited a marked reduction in shape parameter from 19.76 to 10.48. Conversely, Group M from 14.80 to 14.12 and Group P from 6.29 to 6.51 remained relatively stable shape parameters. Characteristic strength of Group P decreased obviously from 140.15 MPa to 116.36 MPa.

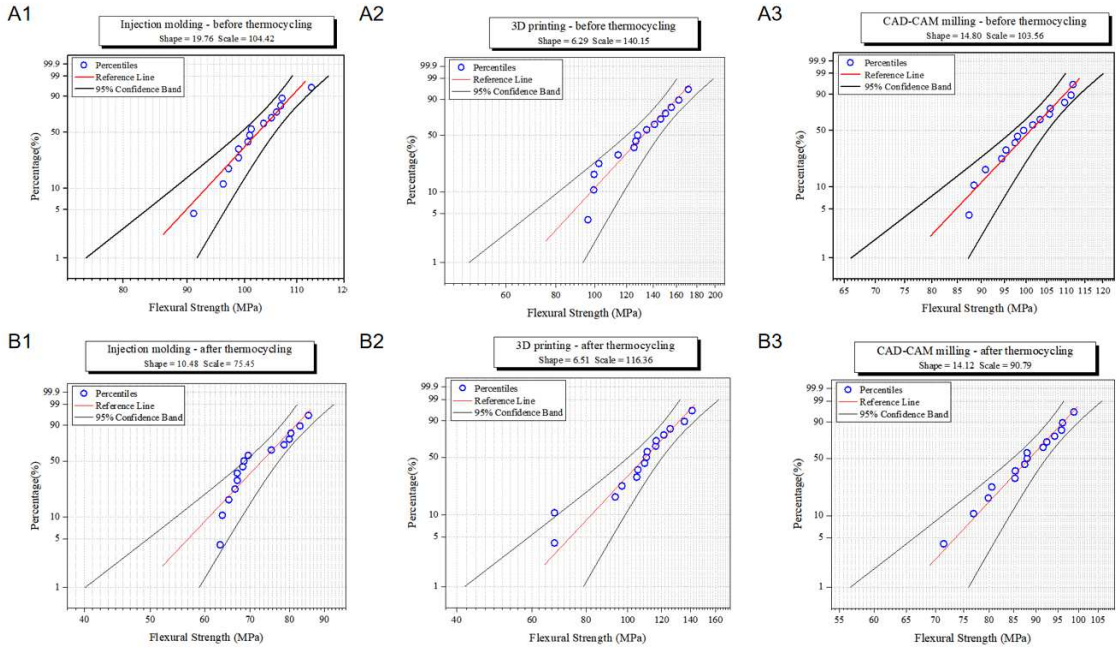


Fig. 5. Weibull probability plots for three fabrication techniques before and after thermocycling. A1) -A3) the distributions of Group I, Group P, and Group M before thermocycling, respectively. B1) -B3) the corresponding distributions after thermocycling, respectively.

3.4 SEM for Mechanical Characterization

At low magnification, Group I and Group M exhibited relatively smooth fracture surfaces with visible river patterns and crack branching, particularly evident at higher magnification before and after thermocycling (Fig. 6A2, A4, C2 and C4), while some fibrous fillers were evident in Group M before and after thermocycling (Fig. 6C1 and C3). Group P containing 19.9 ± 1.1% nanoparticles presented comparatively rougher and more irregular fracture surfaces (Fig. 6B2 and B4). At high magnification, Group M exhibited obvious hole defects (Fig. 6C2 and C4). Besides, the fracture surfaces of

Group P were characterized by apparent particulates before thermocycling (Fig. 6B2), which diminished significantly after thermocycling (Fig. 6B4).

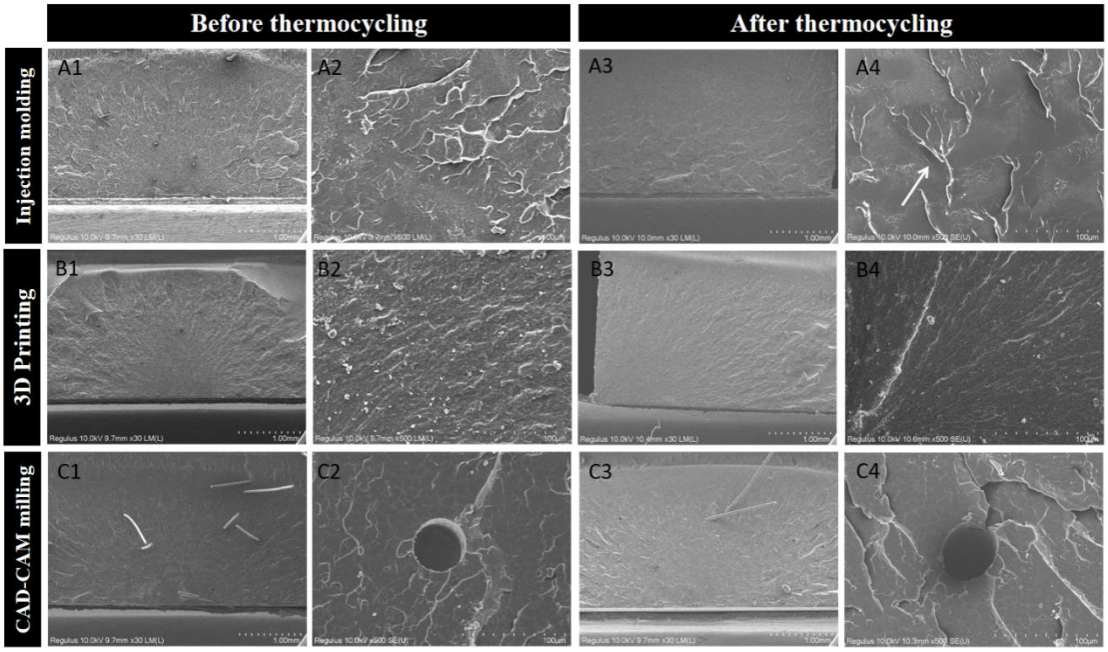


Fig. 6. SEM images for three fabrication techniques before and after thermocycling. A1) -A4) belong to Group I, B1) -B4) to Group P, C1) -C4) to Group M.

3.5 Water contact angle

The results were presented in Fig. 7. Both Group I and Group P exhibited average contact angles of approximately 105.4° and 113.0°, respectively. Group M showed an average contact angle of approximately 93.6°. Statistical analysis revealed that the contact angle of Group M was significantly lower than that of Group I and Group P ($p < 0.05$). There were no statistical significance between Group I and Group P ($p > 0.05$).

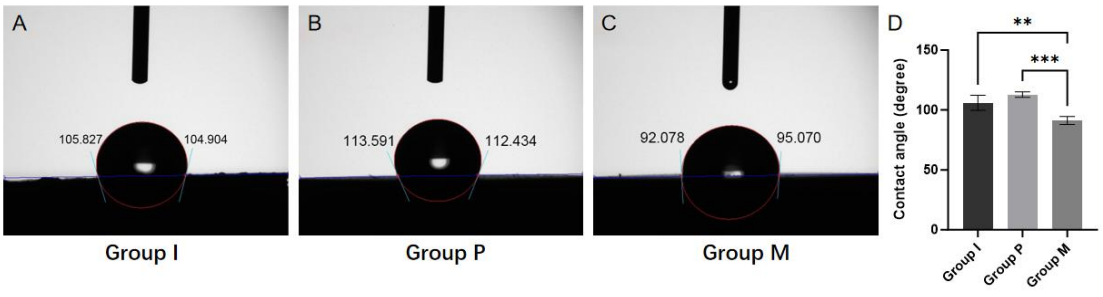


Fig. 7. Representative images of water droplets on PMMA specimens of three fabrication techniques. A) for Group I, B) for Group P, C) for Group M. D) Corresponding statistical chart for quantitative analysis of contact angle.

3.6 Surface Roughness and Topographic Analyses

There were no significant differences in the arithmetic average roughness (Ra) of three groups, with 0.28 ± 0.09 μm for Group I, 0.23 ± 0.07 μm for Group P, and 0.21 ± 0.05 μm for Group M ($p > 0.05$). Surface area difference (SAD)(24) was the ratio of the deviation between the measured area and the scanned area to the scanned area. $SAD = (Measured\ area - Scanned\ area)/Scanned\ area \times 100\%$

Group P exhibited the highest SAD of 501.20 ± 45.15 %, followed by Group I of 476.23 ± 29.95 %, whereas Group M presented the lowest of 471.51 ± 37.40 %. There were no statistically significant differences among groups ($p > 0.05$) (Table 4).

Table 4. The Arithmetic Average Roughness (Ra, μm) and Surface Area Difference (SAD, %) among the PMMA from three fabrication techniques

Group	N	Ra		SAD	
		Mean ± SD	*P* Value	Mean ± SD	*P* Value
Group I	6	0.28 ± 0.09		476.23 ± 29.95	
Group P	6	0.23 ± 0.07	0.195	501.20 ± 45.15	0.372
Group M	6	0.21 ± 0.05		471.51 ± 37.40	

As shown in the surface topography, Group I and Group M presented smooth and homogeneous surface topography, demonstrating a relatively flat surface (Fig. 8A1, A2, C1 and C2). Group P exhibited a uniformly distributed granular micro-texture with frequent sharp peak-and-valley fluctuations (Fig. 8B1 and B2).

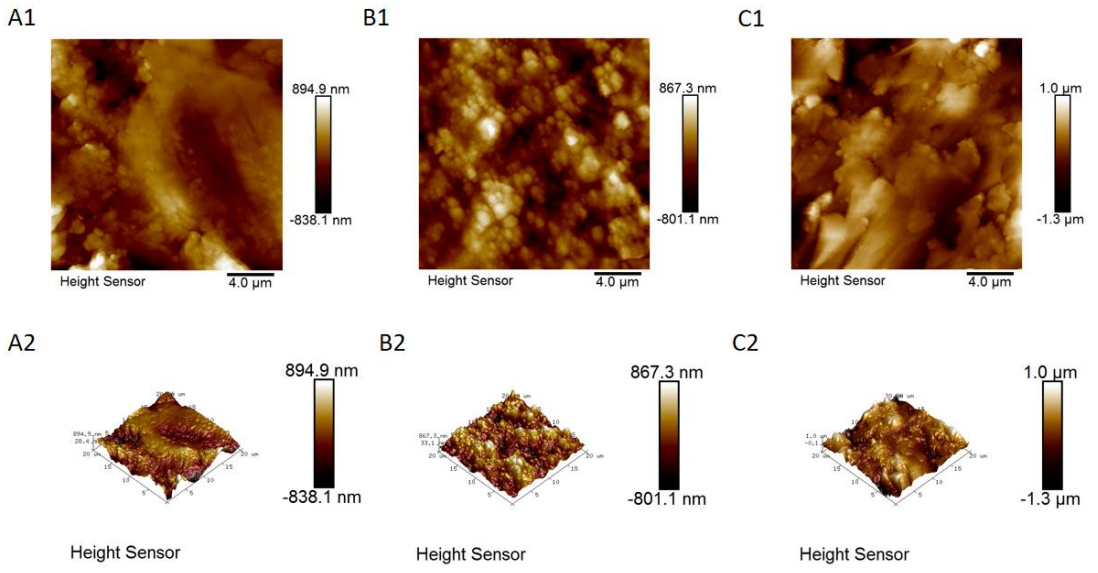


Fig. 8. Representative surface topographic images for PMMA from three fabrication techniques. A1) -A2) height sensor images of Group I, B1) -B2) of Group P, C1) -C2) of Group M. A1) -C1) the two-dimensional topographic images, A2) -C2) the corresponding 3D topographic images.

3.6 Microbial colonization and SEM

The colony counting showed that three groups of specimens exerted different effects on the surface colonization of *C. albicans* and *S. oralis*. For *C. albicans*, Group P presented the highest number of colonies, while Group M exhibited the lowest, with Group I falling in between. Quantitative analysis revealed that the CFU counts of both Group M and Group I were significantly lower than the count of Group P ($p < 0.05$). The count of Group M was significantly lower than that of Group I, indicating that CAD/CAM milling inhibited the colonization or proliferation of *C. albicans* ($p < 0.05$). For *S. oralis*, Group P and Group M showed higher colony counts with no significant difference between them（$p > 0.05$）, while the CFU count of Group I substantially decreased and was significantly lower than those of both the Group P and Group M ($p < 0.05$) (Fig. 9).

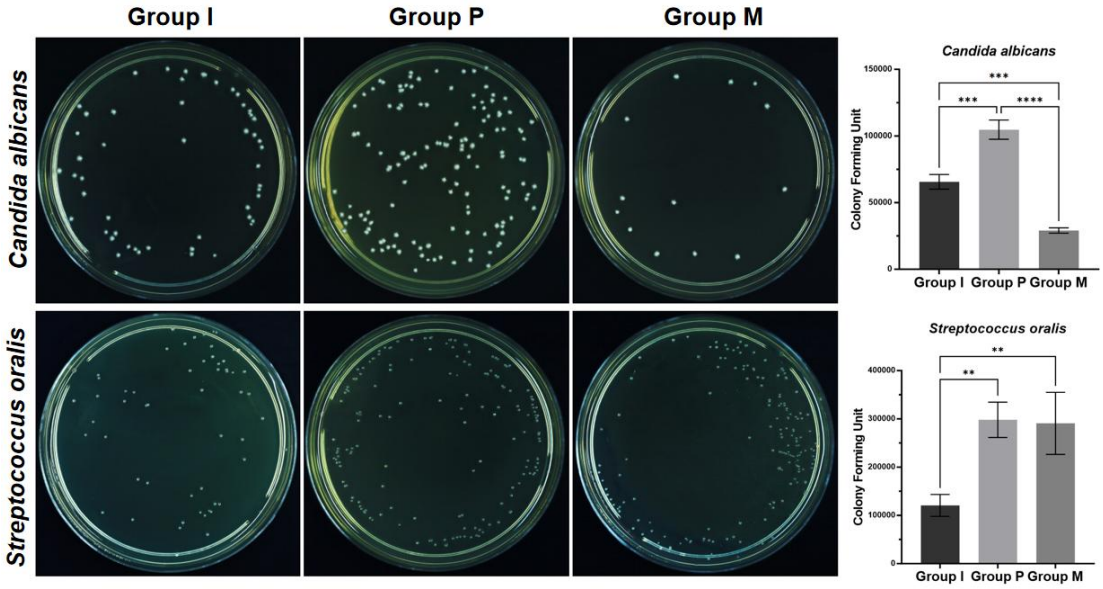


Fig. 9. CFU counts of *C. albicans* and *S. oralis* for three fabrication techniques. Representative photographs of CFU of *C. albicans* and *S. oralis* inoculated on the surface of materials prepared via different processing methods after 24 hours of incubation. Corresponding statistical chart for quantitative analysis of CFU.

At high magnification, oval yeast cells with yeast, pseudohyphae, or true hyphae growth of *C. albicans* were clearly observed on the surfaces of all three groups (Fig. 10A1, A2, B2, C1 and C2). Meanwhile, *S. oralis* were observed as spherical to ovoid cocci arranged in pairs or characteristic long chains (Fig. 10A3, A4, B3, B4, C3 and

C4). Silica fillers could be seen in Fig 10.B2 and machining marks were visible in Fig. 10C1.

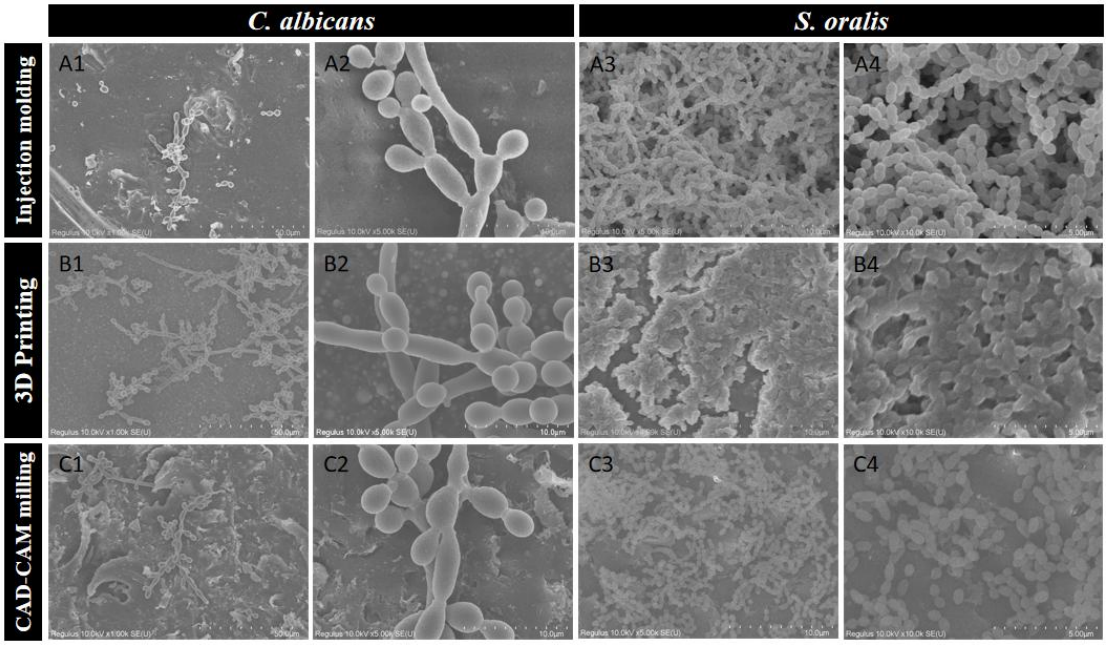


Fig. 10. SEM images of *C. albicans* and *S. oralis* colonization on PMMA specimens fabricated by three fabrication techniques. A1) -A4) belong to Group I, B1) -B4) to Group P, C1) -C4) to Group M.

4. Discussion

This study compared the mechanical properties and microbial colonization of three complete denture fabrication techniques, including 3D printing, CAD/CAM milling and injection molding. The results revealed that the flexural strength of Group I decreased greatly after thermocycling. Besides, Group P exhibited the highest flexural strength before thermocycling. Moreover, the flexural strength and flexural modulus of Group M remained the most stable among groups. When it comes to microbial colonization, Group P showed the highest number of colonies for *C. albicans* and *S. oralis*. These results rejected the null hypothesis and demonstrated that there were mechanical and microbial differences among the PMMA fabricated by different techniques in this study.

4.1 Effects of Fabrication Techniques on Flexural Strength and Weibull Distribution

All the PMMA resins of three groups met the minimum clinical strength requirements of over 65 MPa in terms of flexural strength before thermocycling (20).

3D printing denture base PMMA exhibited the highest flexural strength in this study, which was different from some early studies (4, 25). This difference may result from variations in compositions of the printing resins used. Group P in this study was incorporated with nano-silica fillers, which formed a rigid skeletal framework within the PMMA polymer matrix to bear external loads and enhance the flexural strength (26, 27). The fillers create a thicker interface layer by restricting the movement of polymer chains. Under external loading, stress is transferred from the polymer matrix to the inorganic fillers through the interface, significantly enhancing the flexural strength of PMMA (28).

The flexural strengths of all PMMA decreased after thermocycling but still met the clinical requirements. The scale parameter of Weibull distribution also declined among all groups. The underlying mechanism may be attributed to that cyclic thermal changes induced internal stresses via non-uniform volumetric expansion and contraction, promoting defect accumulation. This process is further explained by moisture-driven hydrolysis by some investigators (22, 29, 30). Compared with injection molding techniques widely used in dental laboratories, 3D printing and CAD/CAM milling PMMA presented lower decrease in flexural strength and scale parameter.

3D printing PMMA exhibited a lower value of Weibull modulus, demonstrating a higher degree of dispersion compared to injection molding and CAD/CAM milling. It is likely attributed to the layer-by-layer DLP technique, where anisotropy appears in specimens because of slight differences in inter-layer bonding and localized uneven photo-curing during polymerization (31). Moreover, FA Morganti et.al found that increasing concentrations of silica fillers increased composite resin properties but limited the printability in the vat-polymerization process (32). CAD/CAM milling technique presented the smallest intensity reduction and the highest data stability, because the discs were prefabricated at high temperatures under unified parameters.

A notable limitation is that the three-point bending test was conducted under dry and ambient laboratory conditions. This fails to account for the plasticization effect that occurs when PMMA absorbs water in the oral environment (33). Future studies should incorporate thermocycling and immersion in artificial saliva to better simulate the oral environment.

4.2 Effect of Fabrication Techniques on Flexural Modulus

The flexural modulus of the denture base reflects its ability to resist deformation when subjected to chewing forces. Before thermocycling, the flexural modulus of all PMMA groups complied with the ISO standard of over 2 GPa (20). After thermocycling, Group I showed an increase in flexural modulus, whereas Group P and Group M experienced a decrease. This discrepancy can be attributed to the incomplete polymerization of Vertex Self-Curing material (34). It is polymerized below the glass transition temperature, resulting in low degrees of polymerization and conversion. The warm environment provided by thermocycling may have compensated for the insufficient curing, thereby promoting secondary polymerization and cross-linking reactions in certain specimens (35). Consequently, the cross-linking structure of the material was further optimized during the thermocycling process, leading to an increase in overall rigidity. A similar phenomenon was observed by Jansen van Vuuren et al., who reported a significant post-thermocycling increase in fracture toughness for Vertex Rapid Simplified heat-cured PMMA, attributing this to thermally-induced post-polymerization of residual monomer.

The flexural modulus of Group M decreased from approximately 2.8 GPa to 2.4 GPa, a decrease smaller than that of Group P. Group P exhibited the most significant decline in flexural modulus after thermocycling, decreasing from approximately 2.8 GPa to roughly 1.7 GPa that was below ISO standard(20). This phenomenon can likely be attributed to two factors. First, the inter-layer structural defects was inherent to the light-curing process. Second, the temperature fluctuations caused by thermocycling process may facilitate the local aggregation of nano-sized SiO_2 fillers, weakening the interface bonding of the filler matrix and generating a negative effect with the pore defects. This finding suggest that the flexural modulus of 3D printing PMMA needs to be optimized in the future.

4.3 Stress-Strain Curve & SEM

The stress-strain curves were drawn based on the three-point bending test in this study instead of tensile test. Because in the oral cavity, denture base resins are predominantly subjected to flexural load rather than pure tensile load during mastication. The stress state induced by three-point bending, characterized by

compression on the upper surface and tension on the lower, more closely simulates the clinical using conditions of maxillary and mandibular dentures. The limitation of this method is that unlike tensile testing, the complex stress state induced by three-point bending does not fully capture the intrinsic properties of PMMA.

The fracture behavior of injection molding and CAD/CAM milling PMMA were characteristic of quasi-brittle fracture in this study. All stress-strain curves of them exhibited elastic deformation, plastic deformation and sudden fracture, which occurred at a strain of about 3%-6%. The river patterns and crack branching were observed at high magnification of SEM images, indicating the PMMA underwent predominate elastic deformation and minimal plastic deformation(36). The elongation at fracture of injection molding shifted from 4%-6% strain before thermocycling to 3%-4% strain after thermocycling, indicating an increased post-thermocycling fracture brittleness. Nejatian et al.(28) demonstrated that self-curing PMMA exhibits a lower degree of conversion and higher residual monomer content, resulting in significantly reduced molecular chain entanglement density and cross-linking uniformity compared to heat-curing systems. In this study, although the environment during thermocycling promoted the secondary polymerization of residual monomers, this non-uniform post-cross-linking reaction introduced additional internal stresses and micro-defects into the pre-existing polymer network, further restricting the mobility of molecular chain segments. Concurrently, the ingress of water molecules during cycling exerted effects of plasticization and hydrolysis on residual monomer-rich regions(33). These changes may explain why the material exhibited increased hardness accompanied by embrittlement, showing no significant variation in flexural modulus.

The curves of 3D printing PMMA before and after thermocycling presented part feature of ductile fracture, while the SEM fracture surface shows a rough layered structure. This is because the printing process creates local variations in crosslinking density during photopolymerization(37), forcing cracks to deflect along interlayer interfaces during propagation(38). Additionally, the added silica filler further contributes to local density differences, enhancing this effect. The curves showed that the yield plateau of 3D printing PMMA decreases after thermocycling. This may be attributed to that thermocycling induced unmatched expansion between silica fillers and PMMA, resulting in micro-debonding and weakening the efficiency of crack deflection(39).

SEM images of CAD/CAM milling PMMA revealed holes within the specimens, indicating that structural defects may also be introduced during the pre-fabrication milling process. Yau et al. pointed out that pressure and temperature changes influenced the heat-cured prefabricated milling disks(40). This highlights the need for manufacturers to optimize processing parameters and enforce strict quality control.

4.4 Surface Features and Microbial colonization

In this study, *C. albicans* and *S. oralis* were selected as the test microorganisms. The former is the primary etiological agent of Candida-associated denture stomatitis, while the latter serve as characteristic pioneer colonizers in initial oral microbial adhesion and biofilm formation.

The highest colonization of *C. albicans* occurred on the surface of 3D printing PMMA, followed by injection molding PMMA, with CAD/CAM milling PMMA the lowest. From the results of the water contact angle, PMMA fabricated by 3D printing and injection molding displayed stronger hydrophobicity than CAD/CAM milling. Some researchers have reported that hydrophobic microorganisms, such as *S. oralis* and *C. albicans*, exhibit a pronounced preference for adhering to more hydrophobic surfaces (38, 39). Therefore, the water contact angle explained why the CAD/CAM milling PMMA showing the lowest colonization of *C. albicans*. Besides, surface topographic images of 3D printing PMMA exhibited a uniformly distributed granular micro-texture with frequent sharp peak-and-valley fluctuations, while images of injection molding PMMA were relatively smooth. This might account for the higher colonization of *C. albicans* on 3D printing PMMA.

S. oralis, as an early bacterial colonizer with a coccal diameter of approximately 0.5-1.25 μm, is smaller than *C. albicans* yeast cells. The quantity results of colonization were similar on 3D printing PMMA and CAD/CAM milling PMMA, and lowest on injection molding PMMA. As can be seen from the SEM images, *S. oralis* could localize not only on the flat area of the surface, but also in the pit area of 3D printing surface and tooling marks of milling surface, where they were protected from shear forces and provided with larger contact area. Injection molding PMMA showed the lowest colonization to *S. oralis*, which could be attributed to its higher residual monomer content inherent of this fabrication technique and this may exert antibacterial effects against *S. oralis* (35).

There were several methodological details that may contribute to the results in this study. First, due to the absence of the recommendation wet milling protocol from the manufacturer, PMMA specimens were fabricated using a dry milling process in preparation phase. Liu et al. (41) demonstrated that dry milling yields a higher water contact angle and greater surface roughness compared to wet milling. These surface alterations may promote bacterial and fungal colonization. Nevertheless, dry milling remains the predominant choice of zirconia and PMMA in dental laboratories because of its efficiency and cleanness. Second, the support structures of the 3D printing PMMA specimens were mechanically removed and subsequently polished during the preparation phase. While this post-processing step is inevitable in routine fabrication, it partly alters the surface topography, potentially influencing the adhesion and colonization of microorganisms. Third, the study lacks a salivary pellicle, which physiologically regulates initial bacterial attachment and surface wettability. Future work should incorporate salivary pellicle formation and multi-species biofilm models to simulate intraoral conditions.

CONCLUSION

1. 3D printing PMMA exhibited the highest initial flexural strength and the flexural modulus of 3D printing PMMA declined significantly after thermocycling and needs to be optimized in the future.

2. CAD/CAM milling PMMA demonstrated the most stable mechanical performance, maintaining the highest post-thermocycling flexural modulus and the highest Weibull shape parameter. However, its clinical adoption may be limited by material cost and fabrication complexity.

3. Conventional injection molding PMMA showed obvious embrittlement and a drastic reduction in reliability after thermocycling.

4. The colonization of *C. albicans* was lowest on the CAD/CAM surfaces, meanwhile injection molding surfaces behaved best in terms of *S. oralis*. 3D printing PMMA surfaces exhibited the highest microbial colonization risk.

Declarations

Ethics approval and consent to participate

This in vitro study did not involve human participants, human data, or animal subjects. No ethics committee approval was required. Not applicable.

Consent for publication

Not applicable.

Availability of data and materials

The datasets generated and/or analysed during the current study are available from the corresponding author on reasonable request.

Competing interests

The authors declare no competing interests.

Funding

Study Supported by the Support Program of the Shanghai Hospital Development Center (Grant No. SHDC12024127) and Shanghai Municipal Health Commission (Grant No. 20244Y0126, 2024ZZ2065 and 2025ZZ1022).

Author contributions

There are eight authors because they all made considerable contributions to this study.

Shuobo Fang: Methodology, Investigation, Writing - original draft, Writing - review & editing, Project administration. Yilin Tu: Investigation, Visualization, Writing - original draft. Nuoyan Xu: Writing – original draft, Visualization. Zhe Shen: Validation, Investigation. Zhicheng Gong: Methodology, Writing - review & editing, Funding acquisition. Jue Wang: Writing - review & editing, Supervision, Funding acquisition. Xueying Wu: Validation, Resources. Taoran Qu: Conceptualization, Supervision, Methodology, Writing - review & editing, Funding acquisition.

Acknowledgements

Not applicable

REFERENCES

1. Anusavice KJ, Shen C, Rawls HR. Phillips' science of dental materials: Elsevier Health Sciences; 2012.
2. Zafar MS. Prosthodontic Applications of Polymethyl Methacrylate (PMMA): An Update. Polymers (Basel). 2020;12(10).
3. Kalberer N, Mehl A, Schimmel M, Müller F, Srinivasan M. CAD-CAM milled versus rapidly prototyped (3D-printed) complete dentures: An in vitro evaluation of trueness. J Prosthet Dent. 2019;121(4):637-43.
4. Yu HJ, Kang YJ, Park Y, Kim H, Kim JH. A comparison of the mechanical properties of 3D-printed, milled, and conventional denture base resin materials. Dent Mater J. 2024;43(6):813-21.
5. Alghazzawi TF. Advancements in CAD/CAM technology: Options for practical implementation. J Prosthodont Res. 2016;60(2):72-84.
6. Khaledi AA, Farzin M, Akhlaghian M, Pardis S, Mir N. Evaluation of the marginal fit of metal copings fabricated by using 3 different CAD-CAM techniques: Milling, stereolithography, and 3D wax printer. J Prosthet Dent. 2020;124(1):81-6.
7. Alghauli MA, Almutairi S, Almuzaini S, Aljohani R, Aljohani W, Alqutaibi AY. Properties and Behavior of Additively Manufactured Provisional Fixed Dental Prostheses: A Systematic Review on 3D Printing Orientations Relative to Applied Materials and Postprocessing. J Esthet Restor Dent. 2025;37(6):1407-18.
8. Watts DC. Light-curing dental resin-based composites: How it works and how you can make it work. Front Dent Med. 2023;4:1108316.
9. Kang MJ, Lim JH, Lee CG, Kim JE. Effects of Post-Curing Light Intensity on the Mechanical Properties and Three-Dimensional Printing Accuracy of Interim Dental Material. Materials (Basel). 2022;15(19).
10. Alhotan A, Yates J, Zidan S, Haider J, Silikas N. Assessing Fracture Toughness and Impact Strength of PMMA Reinforced with Nano-Particles and Fibre as Advanced Denture Base Materials. Materials (Basel). 2021;14(15).
11. Khattar A, Alghafli JA, Muheef MA, Alsalem AM, Al-Dubays MA, AlHussain HM, et al. Antibiofilm Activity of 3D-Printed Nanocomposite Resin: Impact of ZrO(2) Nanoparticles. Nanomaterials (Basel). 2023;13(3).
12. Kim KW, Kim SY, Kim S-A, Jang H-W, Lee K-W, Lee Y-S. Four Different Build Angles in 3D-Printed Complete Denture Bases: A Comparative In Vitro Study. Applied Sciences. 2024.
13. Singh RD, Gautam R, Siddhartha R, Singh BP, Chand P, Sharma VP, et al. High performance liquid chromatographic determination of residual monomer released from heat-cured acrylic resin. An in vivo study. J Prosthodont. 2013;22(5):358-61.
14. Wuersching SN, Manghofer D, Stawarczyk B, Gueth JF, Kollmuss M. Surface Properties of Dental Materials Influence the In Vitro Multi-Species Biofilm Formation. Polymers (Basel). 2026;18(2).
15. Del Hougne M, Mitzscherling A, Ewald A, Schilling T, Stahlhut P, Gbureck U, et al. In Vitro Biofilm Formation on 3D-Printed, Milled, and Conventionally Manufactured Denture Base Resins.

Bioengineering (Basel). 2026;13(4).
16. Gad MM, Abualsaud R, Khan SQ. Hydrophobicity of Denture Base Resins: A Systematic Review and Meta-analysis. J Int Soc Prev Community Dent. 2022;12(2):139-59.
17. Lueyar TK, Karygianni L, Attin T, Thurnheer T. Dynamic interactions between Candida albicans and different streptococcal species in a multispecies oral biofilm. Microbiologyopen. 2023;12(5):e1381.
18. Koujan A, Aggarwal H, Chen PH, Li Z, Givan DA, Zhang P, et al. Evaluation of Candida albicans Adherence to CAD-CAM Milled, 3D-Printed, and Heat-Cured PMMA Resin and Efficacy of Different Disinfection Techniques: An In Vitro Study. J Prosthodont. 2023;32(6):512-8.
19. Hassan SA, Beleidy M, El-Din YA. Biocompatibility and Surface Roughness of Different Sustainable Dental Composite Blocks: Comprehensive In Vitro Study. ACS Omega. 2022;7(38):34258-67.
20. ISO 20795-1:2013. Dentistry — Base polymers Part 1: Denture base polymers. Geneva: International Organization for Standardization; 2013.
21. Lawson NC, Safadi Y, Alford A, Aggarwal H, Bora PV, Lawson TJ, et al. Flexural strength, fracture toughness, translucency, stain resistance, and water sorption of 3D-printed, milled, and conventional denture base materials. J Prosthodont. 2026;35(4):553-60.
22. Osman RB, Khoder G, Fayed B, Kedia RA, Elkareimi Y, Alharbi N. Influence of Fabrication Technique on Adhesion and Biofilm Formation of Candida albicans to Conventional, Milled, and 3D-Printed Denture Base Resin Materials: A Comparative In Vitro Study. Polymers (Basel). 2023;15(8).
23. Grubbs FE. Sample Criteria for Testing Outlying Observations. The Annals of Mathematical Statistics. 1950;21(1):27-58.
24. Siegel J, Grossberger D, Pryjmaková J, Šlouf M, Švorčík V. Laser-Promoted Immobilization of Ag Nanoparticles: Effect of Surface Morphology of Poly(ethylene terephthalate). Nanomaterials (Basel). 2022;12(5).
25. Vincze ZÉ, Nagy L, Cavalcante BGN, Gede N, Hegyi P, Bányai D, et al. Milling has superior mechanical properties to other fabrication methods for PMMA denture bases: a systematic review and network meta-analysis. Dental materials. 2025;41(4):366-82.
26. Balos S, Pilic B, Markovic D, Pavlicevic J, Luzanin O. Poly (methyl-methacrylate) nanocomposites with low silica addition. The Journal of prosthetic dentistry. 2014;111(4):327-34.
27. Zhang Z, Chen D. Consideration of Orowan strengthening effect in particulate-reinforced metal matrix nanocomposites: A model for predicting their yield strength. Scripta materialia. 2006;54(7):1321-6.
28. Nejatian T, Nathwani N, Taylor L, Sefat F. Denture base composites: Effect of surface modified nano-and micro-particulates on mechanical properties of polymethyl methacrylate. Materials. 2020;13(2):307.
29. Gad MM, Rahoma A, Abualsaud R, Al-Thobity AM, Akhtar S, Siddiqui IA, et al. Influence of artificial aging and ZrO2 nanoparticle-reinforced repair resin on the denture repair strength. Journal of Clinical and Experimental Dentistry. 2020;12(4):e354.
30. Çakmak G, Donmez MB, Akay C, Abou-Ayash S, Schimmel M, Yilmaz B. Effect of thermal cycling on the flexural strength and hardness of new-generation denture base materials. Journal of prosthodontics. 2023;32(S1):81-6.
31. Gojzewski H, Guo Z, Grzelachowska W, Ridwan MG, Hempenius MA, Grijpma DW, et al. Layer-by-Layer Printing of Photopolymers in 3D: How Weak is the Interface? ACS Appl Mater Interfaces. 2020;12(7):8908-14.

32. Morganti FA, Zattera ACA, de Souza Balbinot G, Della Bona A, Collares FM. Influence of silica nanoparticle concentration on 3-dimensional–printed resin-based composite. JADA Foundational Science. 2026;5:100059.
33. Silva CdS, Machado AL, Chaves CdAL, Pavarina AC, Vergani CE. Effect of thermal cycling on denture base and autopolymerizing reline resins. Journal of Applied Oral Science. 2013;21(3):219-24.
34. Ko JW, Sakong J, Kang S. Cytotoxicity of dental self-curing resin for a temporary crown: an in vitro study. J Yeungnam Med Sci. 2023;40(Suppl):S1-s8.
35. Urban VM, Machado AL, Vergani CE, Giampaolo ET, Pavarina AC, de Almeida FG, et al. Effect of water-bath post-polymerization on the mechanical properties, degree of conversion, and leaching of residual compounds of hard chairside reline resins. Dent Mater. 2009;25(5):662-71.
36. Ben Said L, Hentati H, Wali M, Ayadi B, Alhadri M. Damage Investigation in PMMA Polymer: Experimental and Phase-Field Approaches. Polymers. 2024;16(23):3304.
37. Zhao Z, Wu D, Chen H-S, Qi HJ, Fang D. Indentation experiments and simulations of nonuniformly photocrosslinked polymers in 3D printed structures. Additive Manufacturing. 2020;35:101420.
38. Štaffová M, Ondreáš F, Svatík J, Zbončák M, Jančář J, Lepcio P. 3D printing and post-curing optimization of photopolymerized structures: Basic concepts and effective tools for improved thermomechanical properties. Polymer testing. 2022;108:107499.
39. Guo C, Li Y, Xu J, Zhang Q, Wu K, Fu Q. A thermally conductive interface material with tremendous and reversible surface adhesion promises durable cross-interface heat conduction. Materials horizons. 2022;9(6):1690-9.
40. Yau W, Cheng Y, Clark R, Chow T. Pressure and temperature changes in heat-cured acrylic resin during processing. Dental materials. 2002;18(8):622-9.
41. Zichuan Liu FW, Jundong Zou, Hailin Liu, Zhaofeng Ma. Influence of different milling conditions on mechanical properties and surface characteristics of denture base resins. BMC Oral Health. 2026.